Available online at www.sciencedirect.com
SCIENCE DIRECT®
Optics Communications 232 (2004) 77–82
OPTICS COMMUNICATIONS
www.elsevier.com/locate/optcom

Creation of a hollow laser beam using self-phase modulation in a nematic liquid crystal

A. Shevchenko [a,*], S.C. Buchter [a], N.V. Tabiryan [b], M. Kaivola [a]

[a] Department of Engineering Physics and Mathematics, Helsinki University of Technology, P.O. Box 2200, HUT FIN-02015, Finland
[b] BEAM Engineering for Advanced Measurements Co., 686 Formosa Ave, Winter Park, FL 32789, USA

Received 26 November 2003; accepted 11 January 2004

Abstract

We present a simple method to convert a Gaussian laser beam into an annular beam using a homeotropically oriented nematic liquid crystal. The method allows creation of a beam with sub-millimeter diameter and a width of a few tens of microns for a propagation distance of more than 10 mm. High spatial gradients in the radial intensity distribution make the beams promising for use in atom trapping and guiding.

PACS: 42.25.Bs; 42.60.−v; 42.60.Jf; 42.65.Jx

Keywords: Hollow laser beams; Self-phase modulation; Nematic liquid crystals

Laser beams with ring-shaped transverse cross-sections have found a variety of applications in science and technology, including trapping and guiding of atoms [1–4], laser manipulation of microscopic dielectric and metal objects [5–7], laser writing and drilling [8,9], measurements of thermal diffusivity [10], and materials testing with the aid of laser-excited acoustic waves [11,12]. The most frequently used beams in these applications are the ones representing a higher-order circularly symmetric mode (TEM_{01^*}) of a laser resonator. Although these beams have a propagation-invariant shape of their intensity profile, the light ring surrounding the on-axis intensity minimum is thick with the width of the ring being comparable in dimension to the beam radius. To concentrate the light power within a thinner ring, one may use a lens-axicon system [3,13,14]. Operation of such systems is based on the fact that, in the focal plane of a lens, a laser beam let through an axicon produces a ring-shaped focal spot. The spot dimensions depend on the focal length, the axicon angle (or refractive-index profile for diffractive axicons [2,15]), and the width of the incident beam. Close to the focal plane, the beam has a high-intensity light wall around a wide dark area. The method has been used with both ordinary

* Corresponding author. Tel.: +35894513166; fax: +35894513155.
E-mail address: andrej@focus.hut.fi (A. Shevchenko).

0030-4018/$ - see front matter © 2004 Elsevier B.V. All rights reserved.
doi:10.1016/j.optcom.2004.01.010

Gaussian and doughnut Laguerre–Gaussian beam illumination. Some other methods, using, e.g., a hollow optical fiber [16], a computer-generated hologram [17], or a liquid crystal with non-uniformly charged, surface-mounted electrodes [18], have also been reported, but they were not aimed at tight radial compression of light.

In this paper, we describe an alternative technique to generate a thin-walled hollow laser beam. The beam is created from a Gaussian beam that undergoes self-phase modulation in a nematic liquid crystal. The experimental setup is shown schematically in Fig. 1. The lens L_1 is used to control the beam diameter at the input of the liquid crystal (LC). If the crystal is located in front of the beam waist, the spatial phase modulation due to the beam convergence has no significant influence on the output field because of the much stronger phase modulation caused by self-focusing [19–22]. At the crystal output, the beam wavefront is deformed in accordance with the nonlinear phase change so that the radius of curvature is negative near the beam axis and positive around it. In the points where the radius is positive, the wave is locally diverging, resembling a wave produced by a beam passed through a ring-shaped aperture. The lens L_2 is chosen to have a low f-number in order to minimize diffraction loss. It creates a magnified image of the "ring aperture" over a longitudinal distance d_{hb} which depends on the beam diameter and power at the crystal cell.

In our experiments, we used a frequency doubled CW Nd:YVO_4 laser (Spectra-Physics Millennia Xs) operating at 532 nm with a beam waist ($1/e^2$) of 1150 μm. Lens L_1 was chosen to have a focal length of 500 mm, so that the focused beam had a waist of 80 μm. The crystal was a 100-μm thick homeotropically oriented nematic liquid crystal with an equivalent nonlinear refractive index of 10^{-5}–10^{-4} cm^2/W [19–21]. For lens L_2, we used a 10× microscope objective with a numerical aperture of 0.25. The output intensity profiles were measured with a CCD camera (Cohu CCIR, 752×582 pixels, 8.6×8.3 μm). Typical measurement results are shown in Fig. 2. The profiles were produced, when the crystal cell was located at the beam waist and the incident-beam power was increased above the self-focusing threshold (approximately 150 mW) to 195 mW. The onset of self-focusing (the Freedericksz transition) was indicated by the appearance of bright diffraction rings [19–21]. To accelerate the transition we first increased the power far above the self-focusing threshold and then set it to the desired value. The

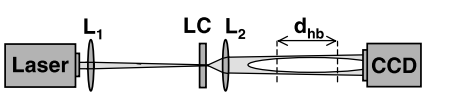

Fig. 1. Experimental setup. The light source is a CW laser and the detector a CCD camera. Lens L_1 is for adjustment of the beam diameter at the input of the nonlinear liquid crystal LC and lens L_2 is for the final beam shaping. Within a certain range (labelled by d_{hb}), the laser field forms a hollow beam with a high peak intensity.

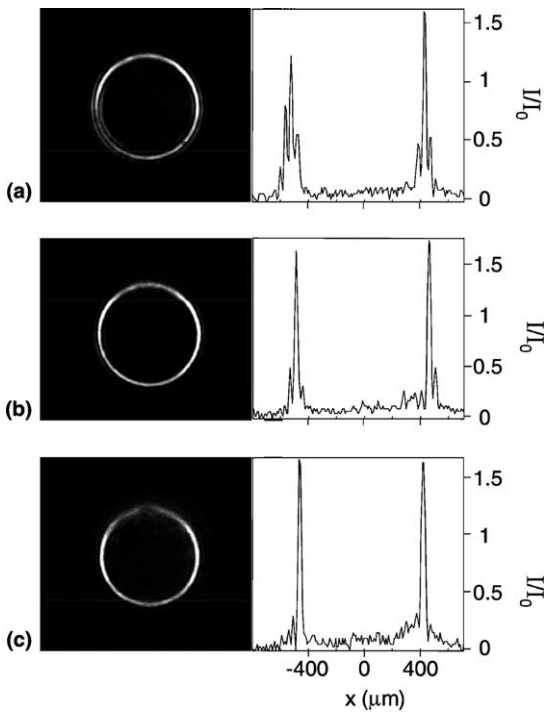

Fig. 2. Transverse cross-sections of a hollow laser beam (on the left) and the corresponding intensity profiles along a horizontal line crossing the beam axis (on the right). The observation planes at (a) and (c) are shifted from that at (b) by −4 and +6 mm, respectively. Before reshaping, the beam had a waist of $W_{LC} = 80$ μm in the crystal plane and $W_{CCD} = 370$ μm in the CCD plane. Its peak intensity in the CCD plane was $I_0 \approx 70$ W/cm^2.

distance between the objective and the crystal was adjusted to provide a nearly constant diameter of the ring. The thinnest ring (see Fig. 2(b)) was observed at a distance of about 8 cm from the objective (the corresponding magnification $M \approx 4.6$). We then measured the beam profiles, shifting the CCD array towards the objective (Fig. 2(a)) and away from it (Fig. 2(c)). The profiles (a) and (b) are separated by 4 mm and (b) and (c) by 6 mm. The ring diameter in Fig. 2(b) is equal to 960 μm and the ring width is 30 μm (FWHM). They both remain approximately unchanged within a distance of about 1 cm. Imperfections of the rings in Fig. 2(a) and (c) are mainly caused by deformations of the original beam profile that was not perfectly symmetric and had some distortions in the tails. In spite of this, we could obtain a rather long and thin-walled "light tube". As shown in Fig. 2, the hollow-beam intensity exceeds 1.5 times the peak intensity of the original Gaussian beam in the CCD plane, which implies an efficient confinement of light in the ring profile. During the beam reshaping, the output power was measured to be constant, which is attributed to a near zero diffraction loss at the objective. The power loss in the setup was caused by reflections of the beam at the glass–air interfaces in both the crystal cell and the objective. The power transmittance of the cell was measured to be 86% and that of the objective 88%. In combination, they transmitted 76% of the light.

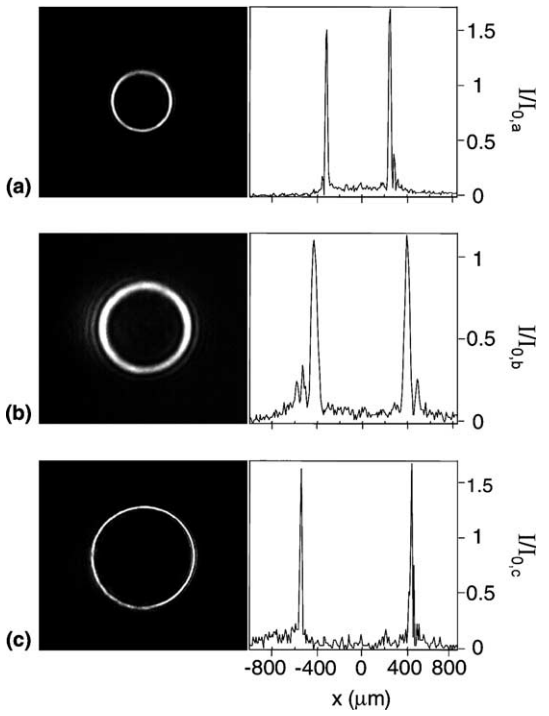

Fig. 3. Transverse-cross-sections of three different hollow beams (on the left) and the corresponding intensity profiles along a horizontal line crossing the beam axis (on the right). The beams are created under different experimental conditions. The parameter values are $P_t = 195$ mW, $W_{LC} = 80$ μm, and $M = 2.7$ in (a), $P_t = 270$ mW, $W_{LC} = 100$ μm, and $M = 4$ in (b), and $P_t = 980$ mW, $W_{LC} = 170$ μm, and $M = 2$ in (c). The peak intensities $I_{0,a}$, $I_{0,b}$, and $I_{0,c}$ of the original Gaussian beams in the CCD plane are 200, 80, and 410 W/cm^2, respectively.

At fixed power P_t and waist W_{LC} of the Gaussian beam at the crystal input, the hollow-beam diameter (D_r), ring width (δ_r), and peak intensity (I_r) can be changed by adjusting the magnification M through shifting the microscope objective. As an example, Fig. 3(a) shows a beam profile obtained under the same conditions as those in Fig. 2, except that the objective was shifted by a few millimeters away from the crystal and the CCD array placed to observe the narrowest light ring. Magnification M in this case is 2.7. The ring has a diameter of 570 μm, a width of 20 μm, and a peak intensity I_r of about 280 W/cm^2. Since this ring is a demagnified version of the ring in Fig. 2(b), the ratio δ_r/D_r for it is approximately the same. The peak intensity, however, is almost three times higher. The ring diameter in this case decreased with the distance from the objective, resulting in a convergent hollow beam.

Creation of beams with different diameters, widths, and peak intensities is possible by a proper selection of the total beam power and the beam diameter in the crystal plane. As an example, Fig. 3(b) shows a thick-ring profile of a beam created when the lens L_1 was shifted by approximately 5 cm towards the crystal (W_{LC} increased to ~100 μm) and the power P_t increased to 270 mW (a value providing a large ring width). The sizes δ_r and D_r in this case are 65 and 830 μm, respectively, while the peak intensity $I_r \approx 100$ W/cm^2 is approximately the same as that in Fig. 2. The thin ring in Fig. 3(c) introduces another example, where the beam was created after shifting the lens

L_1 by a few centimeters more towards the crystal ($W_{LC} \approx 170$ μm) and setting the power to 980 mW. The peak intensity I_r in this case is about 660 W/cm^2, and the beam dimensions are $\delta_r \approx 20$ μm and $D_r = 970$ μm. The ratio δ_r/D_r is equal to 0.02. To create this ring, we compensated for a small ellipticity in the original beam profile by using a cylindrical lens with a long focal length placed in front of the crystal cell. This narrow ring remained undisturbed only within a few millimeters of the beam length. The thick ring of Fig. 3(b), on the other hand, was practically unchanged over the beam length of several centimeters.

To explain the experimental results and give a theoretical description of the method, we calculated the image field on the right-hand side of the lens L_2 within the hollow-beam range marked in Fig. 1. Since the object plane is in this case located in front of the crystal cell, we calculated a virtual object field that, propagating toward the lens in free space, would result in the same field in the image plane as the real self-phase modulated field. To calculate the complex amplitude of the virtual object field, we used Fresnel diffraction integral written in cylindrical coordinates [23]:

$$U(z,\xi) = \frac{2\pi\sqrt{I_p}}{\lambda z}\int_0^\infty \rho\,\mathrm{d}\rho \exp\left(-\frac{\rho^2}{W_{LC}^2} + \mathrm{j}\left(\frac{\pi\rho^2}{\lambda z} + \varphi(\rho)\right)\right) J_0\left(\frac{2\pi\xi\rho}{\lambda z}\right), \quad (1)$$

where the optical axis z (co-directed with the light propagation) is chosen to have the origin in the plane of the crystal's back facet, and the calculations are performed for negative z. The radial coordinate at $z = 0$ is denoted by ρ, and that in the plane of interest by ξ. The field at the crystal output is assumed to be known and described by $U(0,\rho) = \sqrt{I_p}\exp[-\rho^2/W_{LC}^2 + \mathrm{j}\varphi(\rho)]$, where I_p is the peak intensity and $\varphi(\rho)$ the phase difference due to self-phase modulation (the incident wave can be assumed to have a planar wavefront). The function J_0 is the zeroth-order Bessel function of the first kind. We assume the phase difference $\varphi(\rho)$ to be described by

$$\varphi(\rho) = \frac{2\pi}{\lambda} L n_2 I_p \exp\left(-\frac{2\rho^2}{W_{LC}^2}\right), \quad (2)$$

where L is the crystal thickness and n_2 the nonlinear refractive index coefficient. We note that, in reality, the phase φ has a more complicated dependence on ρ, I_p, W_{LC}, and L, especially near the Freedericksz transition [19,22]. However, the assumed form of φ can still provide an accurate qualitative description [19,20]. The virtual-field intensity is found as $I(z,\xi) = |U(z,\xi)|^2$. With the parameter values used to create the beams in Figs. 2 and 3(a), which are $I_p = 1.8 \times 10^3$ W/cm^2 (the intensity inside the crystal), $W_{LC} = 80$ μm, and $L = 100$ μm, numerical integration yields the virtual-field intensity distribution $I(z,\xi)$ shown in Fig. 4, when n_2 is set to 2.3×10^{-5} cm^2/W. Fig. 4(a) illustrates the longitudinal cross-section of the virtual-field intensity profile in the Fresnel zone for z in between −1.6 and −0.52 mm. The field intensity is seen to be concentrated around a conical surface with the apex positioned on the optical axis. When z becomes smaller than about −1 mm, the transverse intensity profile of the virtual field starts to split into diffraction rings seen also in Fig. 2(a). The intensity profile along the vertical line at $z = -1.1$ mm is shown in Fig. 4(b). The parameters D_v and δ_v for this profile are equal to 230 and 7 μm, respectively. When the apex of the conical surface is at the front focal plane of the imaging lens L_2 (Fig. 4(c)), the image of the virtual field constitutes a *cylindrical* light surface of radius $D_r = MD_v$ with $M = f/a$. The distance a turns out to be 3 mm. Magnification M for creation of the beam of Fig. 2 was 4.6. Using this value for M, we obtain $D_r \approx 1$ mm and $\delta_r \approx 30$ μm, which are close to the values obtained in the experiment. Within a distance d_v (see Fig. 4(c)), the calculated virtual field has nearly constant peak intensity. In ray-optics approximation, the corresponding distance d_{hb} of the image is equal to $f^2 d_v/(a^2 - d_v^2)$, which for $d_v^2 \ll a^2$ yields $d_{hb} \approx M^2 d_v$. The effective hollow-beam length is therefore equal to $d_{hb} \approx 4.6^2 \times 0.5$ mm ≈ 10 mm, which again agrees well with the experiment. Shifting the lens L_2 further from the crystal results in a smaller magnification and, in addition, in a convergence of the hollow beam (the case with the beam of Fig. 3(a)). If, on the other hand, the lens is shifted towards the crystal, the magnification M becomes larger and the beam diverges.

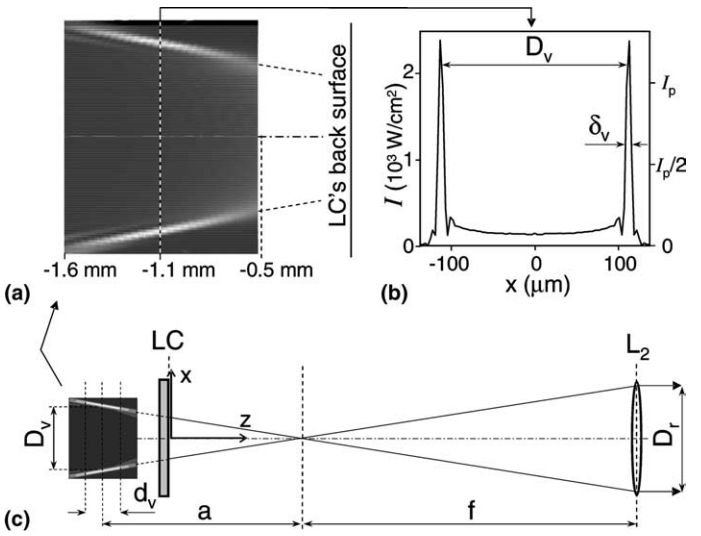

Fig. 4. The calculated virtual-field intensity profiles in a plane containing the axis z (a) and in a perpendicular plane at $z = -1.1$ mm along a radial direction (b). The parameters I_p and W_{LC} are chosen to be 1.8×10^3 W/cm^2 and 80 μm, respectively. Figure (c) shows where the lens L_2 should be positioned to produce a hollow beam with a constant diameter.

Calculating the virtual fields for different values of the original beam intensity I_p in the range 1.3×10^3–2.4×10^3 W/cm^2, we found that the diameter D_v does not depend on I_p, but the distance a scales approximately as $1/I_p$. Since $M = f/a$ is proportional to I_p, the diameter $D_r = D_v M$ of the hollow beam increases together with I_p (the lens L_2 is supposed to be always aligned for creation of a beam with a constant diameter). The calculated parameters δ_r and d_{hb} show a weaker dependence on I_p. The same can be said about the peak intensity I_r. In order to change I_r in a wide range, one has to change the beam diameter at the crystal input. As an example, we calculated the virtual-field intensity $I(z, \xi)$ for the parameters $I_p = 2 \times 10^3$ W/cm^2 and $W_{LC} = 170$ μm used to obtain the thin light ring of Fig. 3(c). The ratio δ_v/D_v obtained matches the experimental value of $\delta_r/D_r = 0.02$, when the coefficient n_2 is set to 3×10^{-5} cm^2/W. The intensity profiles, a longitudinal profile in the Fresnel zone and a transverse one in the plane where the field has the maximum peak intensity (at $z = -3.5$ mm), are shown in Fig. 5(a) and (b), respectively. The distance a is in this case equal to 8.5 mm and the diameter D_v to 500 μm. With the experimental value for the magnification, $M \simeq 2$, the hollow-beam diameter D_r is equal to 1 mm and δ_r is 20 μm. The effective hollow-beam length is calculated to be $d_{hb} = M^2 d_v \approx 4$ mm, where d_v is taken to be equal to 1 mm. The peak intensity $I_r = I_v/M^2$ is now 875 W/cm^2, which is in good agreement with the experiment. In fact, the values of I_p of the Gaussian beam inside the crystal are close to each other in all the examples discussed above (it is mostly determined by the crystal properties). The same is valid for the intensity I_v of the calculated virtual field. Thus, as $I_r = I_v/M^2$, the way to adjust I_r is in altering M. The magnification M required to keep the beam non-diverging is determined by a, and a is approximately proportional to W_{LC}. Hence, for rough estimations, the hollow-beam intensity I_r can be considered to be $I_r \propto W_{LC}^2$. Creation of thick-walled beams (like the one shown in Fig. 3(b)) requires lowering of I_p close to the Freedericksz transition. In this case, the calculated parameters show more deviations from the results of the experiments.

In conclusion, we have demonstrated the creation of a thin-walled hollow laser beam, using a highly nonlinear nematic liquid crystal. An optical system needed to produce beams of different sizes

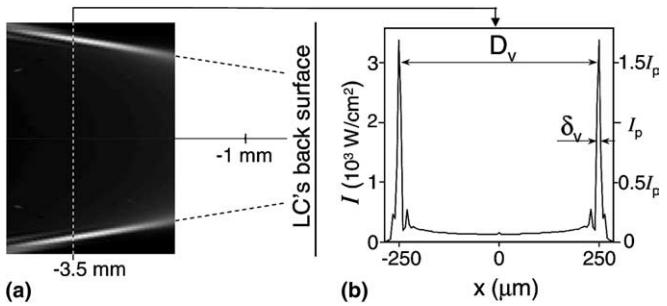

Fig. 5. The virtual-field intensity profiles in a plane containing the axis z (a) and in a perpendicular plane at $z = -3.5$ mm along a radial direction (b). The parameters I_p and W_{LC} are chosen to be 2×10^3 W/cm^2 and 170 μm, respectively.

and peak intensities is (1) simple, (2) not sensitive to alignment of optical elements (the light-induced phase grating is a priory perfectly aligned), (3) able to produce non-diverging hollow beams (as well as diverging or converging ones), and (4) it works equally well at different laser wavelengths. We have also described the results obtained using Fresnel diffraction theory and have presented some general rules for adjusting the beam parameters.

Acknowledgements

We acknowledge financial support from the Academy of Finland.

References

[1] M. Hammes, D. Rychtarik, V. Druzhinina, U. Moslener, I. Manek-Hönninger, R. Grimm, J. Mod. Opt. 47 (2000) 2755.
[2] R. Ozeri, L. Khaykovich, N. Friedman, N. Davidson, J. Opt. Soc. Am. B 17 (7) (2000) 1113.
[3] Y. Song, D. Milam, W.T. Hill III, Opt. Lett. 24 (24) (1999) 1805.
[4] K. Bongs, S. Burger, S. Dettmer, D. Hellweg, J. Arlt, W. Ertmer, K. Sengstock, Phys. Rev. A 63 (2001) 031602(R).
[5] G. Roosen, C. Imbert, Opt. Commun. 26 (3) (1978) 432.
[6] L. Paterson, M.P. MacDonald, J. Arit, W. Sibbett, P.E. Bryant, K. Dholakia, Science 292 (5518) (2001) 912.
[7] M. Gu, D. Morris, J. Appl. Phys. 91 (3) (2002) 1606.
[8] R.B. Charters, B. Luther-Davies, F. Ladouceur, IEEE Photon. Technol. Lett. 11 (12) (1999) 1617.
[9] R.B. Barber, Laser optical apparatus for cutting holes, US Patents 3,419,321, December 1968.
[10] J.C. Kim, D.J. Kim, D.S. Kim, S.W. Kim Troitsky, O. Yu, Int. J. Thermophys. 22 (3) (2001) 933.
[11] C.K. Jen, P. Cielo, X. Maldague, K. El-Assal, J. Am. Ceram. Soc. 68 (6) (1985) C146.
[12] X. Wang, M.G. Littman, J.B. McManus, M. Tadi, Y.S. Kim, A. Askar, H. Rabitz, J. Appl. Phys. 80 (8) (1996) 4274.
[13] I. Manek, Yu.B. Ovchinnicov, R. Grimm, Opt. Commun. 147 (1998) 67.
[14] J. Arlt, R. Kuhn, K. Dholakia, J. Mod. Opt. 48 (5) (2001) 783.
[15] A. Kaplan, N. Friedman, N. Davidson, J. Opt. Soc. Am. B 19 (6) (2002) 1233.
[16] J. Yin, H.R. Noh, K.I. Lee, K.H. Kim, Y.Z. Wang, W. Jhe, Opt. Commun. 138 (1997) 287.
[17] M.A. Clifford, J. Arlt, J. Courtial, K. Dholakia, Opt. Commun. 156 (1998) 300.
[18] D. Ganic, X. Gan, M. Gu, Opt. Lett. 27 (15) (2002) 1351.
[19] J.J. Wu, S.H. Chen, J.Y. Fan, G.S. Ong, J. Opt. Soc. Am. B 7 (6) (1990) 1147.
[20] I.C. Khoo, J.Y. Hou, T.H. Liu, P.Y. Yan, R.R. Michael, G.M. Finn, J. Opt. Soc. Am. B 4 (6) (1987) 886.
[21] N.V. Tabiryan, B.Ya. Zel'dovich, A.V. Sukhov, Mol. Cryst. Liquid Cryst. 136 (1) (1986) 139.
[22] M.A. Bolshtyansky, N.V. Tabiryan Zel'dovich, B. Ya, Opt. Lett. 22 (1) (1997) 22.
[23] J.W. Goodman, Introduction to Fourier Optics, McGraw-Hill, Singapore, 1996.